Aerosol Science and Technology
Publication details, including instructions for authors and subscription information:
http://www.informaworld.com/smpp/title~content=t713656376

Direct Deposition of Aerosol Particles on an ATR Crystal for FTIR Spectroscopy Using an Electrostatic Precipitator

J. Ofner [a]; H. -U. Krüger [ab]; C. Zetzsch [ab]; H. Grothe [c]
[a] Atmospheric Chemistry Research Laboratory, BayCEER, University of Bayreuth, Bayreuth, Germany [b] Fraunhofer-Institute of Toxicology and Experimental Medicine, Hannover, Germany [c] Institute of Materials Chemistry, Vienna University of Technology, Vienna, Austria

First Published on: 01 August 2009

To cite this Article Ofner, J., Krüger, H. -U., Zetzsch, C. and Grothe, H.(2009)'Direct Deposition of Aerosol Particles on an ATR Crystal for FTIR Spectroscopy Using an Electrostatic Precipitator',Aerosol Science and Technology,43:8,794 — 798
To link to this Article: DOI: 10.1080/02786820902946612
URL: http://dx.doi.org/10.1080/02786820902946612

Aerosol Science and Technology, 43:794–798, 2009

ISSN: 0278-6826 print / 1521-7388 online
DOI: 10.1080/02786820902946612

Direct Deposition of Aerosol Particles on an ATR Crystal for FTIR Spectroscopy Using an Electrostatic Precipitator

J. Ofner,[1] H.-U. Krüger,[1,2] C. Zetzsch,[1,2] and H. Grothe[3]

[1]*Atmospheric Chemistry Research Laboratory, BayCEER, University of Bayreuth, Bayreuth, Germany*
[2]*Fraunhofer–Institute of Toxicology and Experimental Medicine, Hannover, Germany*
[3]*Institute of Materials Chemistry, Vienna University of Technology, Vienna, Austria*

An electrostatic precipitator (ESP) has been developed for collecting aerosol samples for attenuated total reflection Fourier transform infrared spectroscopy (ATR-FTIR) from an aerosol chamber. The ESP deposits the aerosol particles directly onto the ATR crystal with high efficiency. The ESP-ATR spectra are observed to agree well with the spectrum of a filter sample, transferred by impression. ZnSe ATR crystals have been found most suitable for electrostatic precipitation due to surface hardness, transmission characteristics and deposition behavior. ESP-ATR-FTIR spectroscopy might be a powerful tool not only for in situ but also for online measurements of aerosols.

INTRODUCTION

FTIR spectroscopy can provide structural and chemical information on organic macromolecules such as components of atmospheric aerosols. However, these samples exhibit high optical density, and therefore, in situ transmission measurements are often hampered by insufficient signal-to-noise ratio while transmission spectroscopy using KBr pellets is much more time consuming (Havers et al. 1998). Reflection techniques are an alternative strategy since they have the inherent advantage of being independent of sample thickness and unlike transmission spectroscopy they avoid the influence of light scattering on the spectral data, which is a source of interference in absorption spectroscopy of opaque samples (Muckenhuber et al. 2007).

ATR spectroscopy is a powerful technique to analyze secondary organic aerosol particle fractions using FTIR. Such spectra are reported in literature for various secondary organic aerosols (Dekermenjian et al. 1999). To perform ATR spectroscopy of organic aerosols, various sample preparation techniques have been described in the literature. Most common is the sampling of atmospheric compounds on filters. These samples are then transferred to the ATR crystal by impression (Ghauch et al. 2006). Rather, no reproducible quantitative measurements are possible because of incomplete transfer of the sample from the filter onto the crystal. Furthermore, misinformation can occur because of the contribution of the filter material to the infrared spectrum. Another possibility would be the use of an impactor to collect atmospheric aerosols on the ATR crystal directly (Allen et al. 1994). This technique allows size dependent measurements but will not allow analyzing the total particle fraction (Johnson et al. 1983). Direct deposition of model aerosol samples by gravimetric deposition onto ATR crystals gave promising results (Zhang et al. 2005). Morrow and Mercer (1964) described a single stage point-to-plate electrostatic precipitator for electron microscopy using field charging to gather and deposit aerosol samples. Some other designs of electrostatic precipitators are reported in literature. Mainelis et al. (2002) describe a precipitator for bio aerosol collection on Agar plates. This ESP consists of 3 components, where charging and precipitating is separated. Fierz et al. (2007) developed a portable ESP for TEM, were charging and deposition is separated. Such a direct deposition technique for atmospheric aerosols on plane surfaces seems a promising alternative to other methods of in situ spectroscopy.

DESIGN OF THE ELECTROSTATIC PRECIPITATOR (ESP) AND EXPERIMENTAL CHARACTERIZATION

To perform ATR-FTIR spectroscopy of organic aerosols from a smog chamber (700 liters, made of borosilicate glass), an ESP was developed based on the concept of a point-to-plane ESP of the Rochester design (Abdel-Salam et al. 2007). It is a single-stage electrostatic precipitator where the same electric field will do both, charge the aerosol particles and deposit them on the crystal. This design was chosen to match the precipitation area to the crystal geometry in an easy way and because of the easy setup of the electric system.

Received 13 October 2008; accepted 7 March 2009.
This work was supported by the Deutsche Forschungsgemeinschaft within the HALOPROC project, by the European Union within the EUROCHAMP project and within the network of excellence ACCENT, and by the Fraunhofer-Gesellschaft.
Address correspondence to H. Grothe, Institute of Materials Chemistry, Veterinaerplatz 1/GA, Vienna A-1210, Austria. E-mail: grothe@tuwien.ac.at

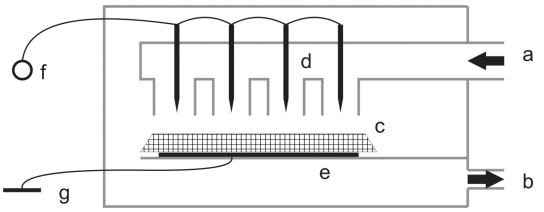

FIG. 1. Design of the ATR-crystal ES: a—aerosol inlet; b—vacuum pump; c—ATR crystal; d—charging electrodes; e—copper electrode; f—high voltage supply; g—ground connection.

The ESP is situated inside a cylindrical glass vessel (70 mm diameter, 160 cm length) wherein the ATR crystal (trapezoidal shape, 52 × 20 × 2 mm) is placed on a sample carrier, made of epoxy. A copper layer on the sample carrier connects to the electric ground (Figure 1e). Four metal needles (curvature-radius of the tip about 30 μm) are mounted inside the inlet tubes and directed to the ATR crystal surface. The needles are surrounded by PVC tubes guiding the divided aerosol flows in parallel towards the crystal surface. With the use of the four PVC tubes, most of the surface of the ATR crystal is covered with the overall aerosol mass. The material of the needles is common steel with no special quality. In normal operation mode the needles are about 1 mm above the crystal. They are connected to a high voltage supply generating an electric field and electrons/ions by corona discharge. The inlet (Figure 1a) is made of Teflon®. It has 8 mm inner diameter and 50 cm length to reach the free volume of the chamber behind the glass connector of the smog chamber, and the outlet is pumped by the aerosol analysis equipment (see below). All inner surfaces of the electrostatic precipitator are non-conductive, except the needles and the ground connection.

CHARACTERIZATION OF THE ELECTROSTATIC PRECIPITATOR

The performance of the ESP was tested towards several operation modi with the three different ATR crystals, Ge, ZnSe, and KRS-5 (Korth Kristalle, Altenholz, Germany) and two insulators (soda lime glass and PVC, 2 mm thick each) were tested for comparison.

For this characterization secondary organic aerosol was produced in the 700 L smog chamber using a reacting mixture of 10 ppm of ozone with 10 ppm of α-pinene. Particle formation to stable aerosol concentrations at about $5{\cdot}10^5$ particles cm^{-3} with volume densities of 7000 μm^3 cm^{-3} took about 15 min. Aerosol particle concentrations were recorded using a TSI 3020 condensation nucleus counter (CNC). A TSI 3071 electrostatic classifier coupled to the CNC was used to determine the aerosol size distribution. Ozone was measured using an UPK 8002 ozone analyzer.

Electrostatic precipitation starts above a certain threshold (Figure 2), and for most if not all materials there is another threshold where formation of additional particles begins. An optimum efficiency of 90% deposition inside the ESP is reached

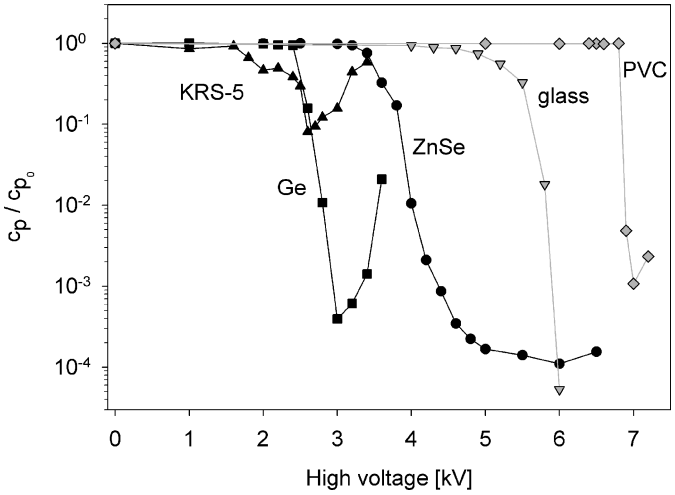

FIG. 2. Deposition behavior of aerosol particles on different ATR crystals and other materials at a flow of 0.3 dm^3 min^{-1}. The remaining proportion of particles [c_p/c_{p0}] is the particle fraction of the aerosol, which is measured by the CNC behind the ESP. The graphs are corrected for the loss of particles by deposition on the smog chamber walls.

at 2.6 kV for KRS-5, of > 99.9% at 3.0 kV for Ge and > 99.99% for ZnSe at > 6 kV. The insulators glass and PVC require much higher voltages for an efficient precipitation. ZnSe is found to be the most suitable material for electrostatic precipitation since it allows rather high deposition efficiency at stable conditions. Furthermore, the spectral throughput between 4000 cm^{-1} and 400 cm^{-1} is rather high. Germanium shows deposition at lower voltages but with not as high rates as ZnSe. With this material particle formation occurs above 3 kV. KRS-5 was not applicable for deposition experiments because only very low deposition rates could be achieved until strong particle formation occurs.

Comparing deposition experiments with the other materials reveals a dependence of the deposition voltage on the permittivity of the material (Table 1, Figure 3). Therefore a characteristic high voltage, where 99% of the aerosol is deposited within the ESP, was determined for each tested material. These values are observed to decrease in almost quadratic dependence on the

TABLE 1
Tested material and its relative permittivity and high voltage of deposition

Material	Rel. permittivity ε_r	High voltage for 99% deposition [kV]
Germanium	16.6[a]	2.8
ZnSe	8.976[a]	4.0
Glass	5–7[b]	5.8
PVC	4.55[c]	6.9

[a]Korth Kristall GmbH.
[b]Soda lime glass; various specifications.
[c]at 1 kHz; *Handbook of Chemistry and Physics* (74th ed., 1993–1994).

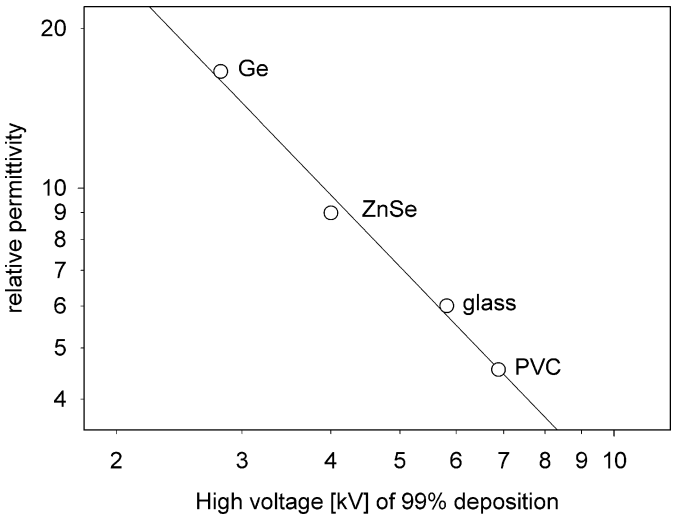

FIG. 3. Dependence of deposition voltage on permittivity of different materials: according to Figure 2 all tested materials (except KRS-5) are plotted with their characteristic high voltage, were 99% of aerosol deposition occurs, against their relative permittivity.

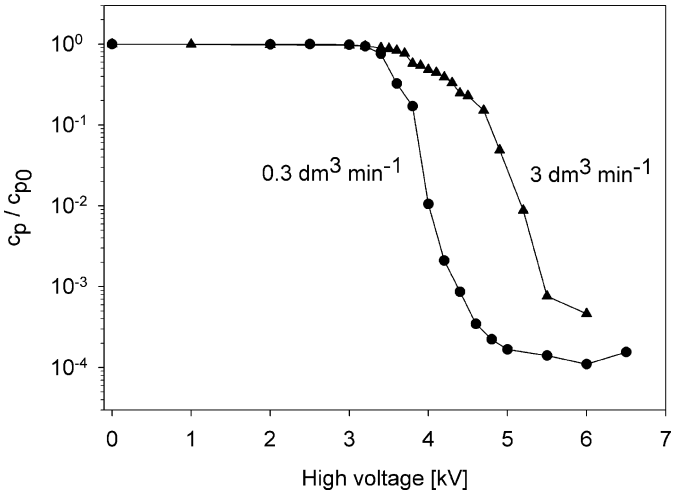

FIG. 4. Deposition behavior of aerosol particles on ZnSe crystals by an order of magnitude different aerosol flows. The remaining amount of particles [c_p/c_{p0}] was determined in the same way as in Figure 2.

permittivity of the materials. As shown with KRS-5 there is a lower limit of the deposition voltage, the voltage above which charging of the aerosol particles takes place. A too high permittivity will not allow deposition because electron emission does not occur at these low voltages. Increasing the high voltage using high permittivities will lead to unwanted side effects such as particle formation or ozone production. The permittivity of the Ge crystal is nearly at the limit of the corona discharge voltage. KRS-5 is below this limit.

The voltage to current characteristic of the ESP was measured with the ZnSe crystal as a substrate. A Keithley 614 electrometer was used to record the current which leaves the ESP from the grounded copper area below the crystal. At 2.3 kV the discharge current starts in the range 1–10 nA. In the region where the ZnSe crystal is operated (3.6–4 kV) the discharge current increases to 5–10 μA in a cubic behavior.

Comparing the collected aerosol mass on the ZnSe crystal to the aerosol mass on a quartz fiber filter after one hour measuring exhibits a deposition efficiency on the crystal only of about 90% at an initial aerosol concentration of $1{\cdot}10^6$ particles cm^{-3}. At these conditions about 39 μg L^{-1} aerosol particles were deposited at a flow rate of 5 cm^{-3} s^{-1}.

An increase of the aerosol flow rate from 0.3 to 3 dm^3 min^{-1} requires a higher deposition voltage to achieve the same deposition efficiency compared to the lower flow rate (Figure 4). The residence time of the aerosol in the region between the ionizing needle tips and the crystal was calculated to be $3{\cdot}10^{-2}$ s for a flow of 0.3 dm^3 min^{-1} and $3{\cdot}10^{-3}$ s for 3 dm^3 min^{-1}.

The ESP was operated with the ZnSe crystal at about 3.6–4.0 kV and at a flow of 0.3 dm^3 min^{-1}. At these conditions, deposition rates of secondary organic aerosol from α-pinene of about 2 μg min^{-1} with a deposition efficiency of more than 95% have been obtained. The deposition efficiency was measured with different aerosol particles with diameters varying from 30–1000 nm. Over the whole range always more than 90% of the particles were deposited (Figure 5).

The deposition behavior of aerosol particles onto the ATR crystal recorded for one hour shows sporadic deposition from the ATR crystal because of local highly charged areas. These sporadic deposition events are below 0.01% of the overall aerosol mass. After 10 minutes 99.9% of the aerosol mass is deposited. The deposited aerosol mass is continuous increasing over a

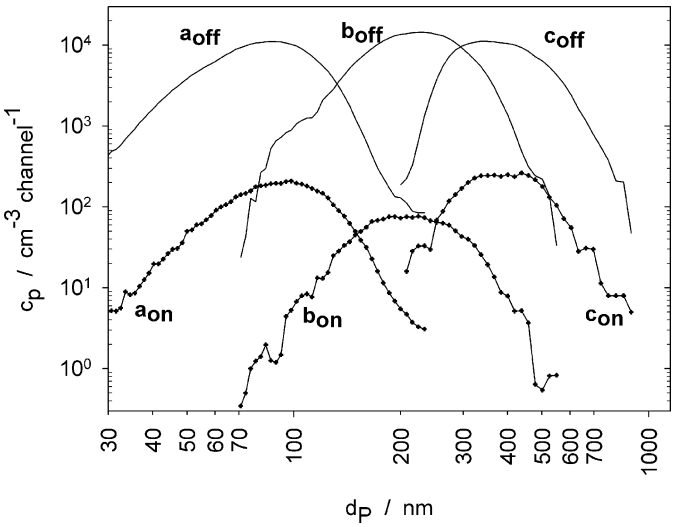

FIG. 5. Deposition of secondary organic aerosol from α-pinene aerosol on a ZnSe ATR-crystal, determined by an electrostatic classifier with CNC. Graphs marked with "a" show experiments using particles with a medium diameter of 90 nm, "b" with 200 nm, and "c" with 400 nm. Graphs with off-indexes were measured at 0 kV voltage of the ESP, graphs with on-indexes at 3.8 kV.

deposition duration of one hour. The ESP exhibits a long-term stability of more than 99.9%.

At material depending voltages (ZnSe: >5 kV, Ge: > 3 kV, KRS-5: > 2.8 kV) we recognized an unwanted side effect: formation of new particles with diameters of about 10 nm was observed before the flashover from the needles to the crystal followed. At these voltages the surface of the ATR crystal was damaged because of sputtering, i.e., metallic particles from the needles were accelerated in the strong electric field hitting the crystal surface.

In these experiments the optimum operation voltage was fixed to 3.6–3.8 kV for the ZnSe crystal. At this voltage of deposition 1 ppm (at 0.3 dm^3 min^{-1}) of ozone was formed due to the electric discharge. In principle, the increasing amount of ozone at higher deposition voltages could be a reason for the new particle formation described above (Keskinen et al. 1986), but control experiments gave no indication.

The ESP can also be operated using positive high voltage. The operation conditions are nearly the same as with negative high voltage. Using positive high voltage causes only a few hundred ppb of ozone. Therefore positive high voltage can be used for aerosols which are sensitive towards reactions with ozone.

FTIR-SPECTRA OF SECONDARY ORGANIC AEROSOL

The formation of secondary organic aerosol and its chemical transformation after reaction with atmospheric trace gases was studied in a smog chamber using infrared spectroscopy. Therefore, an electrostatic precipitator was constructed to analyze the formed or reacted aerosol particles. The organic aerosol was produced the way described above.

Characteristic deposition patterns of the secondary organic aerosol cover the ATR crystal (Figure 6). The FTIR-ATR spectrum of secondary organic aerosol, formed from α-pinene after reaction with ozone and deposited on the ATR crystal using electrostatic precipitation does not observably differ from the FTIR-ATR spectrum of the same aerosol generated by using a Teflon® filter to accumulate the sample (Figure 7). No influence of the additional 1 ppm ozone (from the ESP) was observed, that might have strongly changed the carboxylic and carbonylic functional group absorptions below 1900 cm^{-1}. Chemical transformation of the aerosol by the electric field has not been observed with

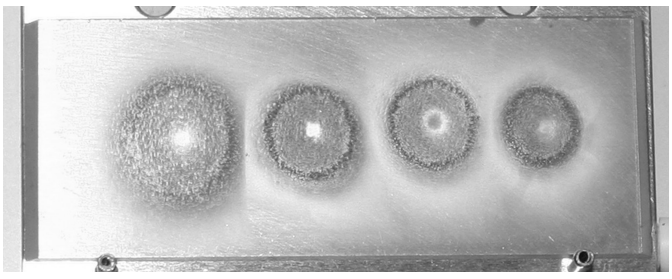

FIG. 6. Photograph of deposited aerosol particles on the ZnSe ATR crystal.

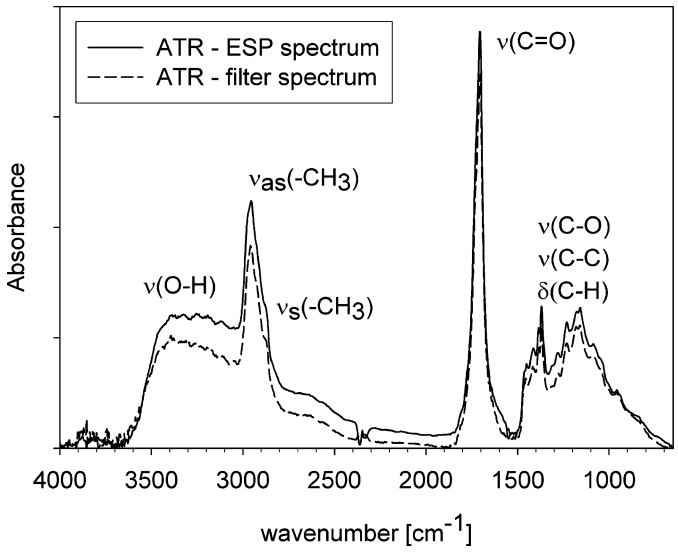

FIG. 7. ATR-FTIR spectra of secondary organic aerosol formed by oxidation of α-pinene with ozone.

these organic aerosol samples, but this effect is possible and must be checked using other kinds of aerosol.

The ATR spectra were recorded using a Bruker IFS 48 FTIR instrument with a Specac 25 reflection ATR optics. The spectral resolution of the infrared spectrometer was adjusted to 4 cm^{-1}, and 512 interferograms with an optical range from 4000 to 600 cm^{-1} were recorded each for background and sample measurement.

The infrared spectrum is similar to former published infrared spectra of secondary organic aerosol from gas to particle conversion of α-pinene (Sax et al. 2005). The broad absorption at 3600–3100 cm^{-1} complies with the O—H stretching vibration ν(O—H). The sharp peak at 2957 cm^{-1} is assigned to the asymmetric C—H stretching vibration of $-CH_3\nu_{as}(-CH_3)$, and the shoulder at 2881 cm^{-1} to the symmetric stretching $\nu_s(-CH_3)$. The strong peak at 1706 cm^{-1} belongs to various C=O stretching vibrations ν(C=O). The rather fine structure below 1500 cm^{-1} complies with the C—O stretching vibrations of various oxygen containing functional groups ν(C—O), next to the C—C stretching vibration ν(C—C) and the C—H rocking or deformation vibration δ(C—H) of the organic structure of the aerosol.

CONCLUSIONS

This electrostatic precipitator allows us to measure ATR-FTIR spectra of aerosols which are directly deposited on the ATR crystal. No manipulations of filters or impactors are needed.

At defined flow and constant voltage quantitative measurements of functional groups are possible (Blando et al. 2001).

The ESP has to be adjusted only one time to the optimum electrostatic field parameters. The permittivity of the used ATR crystal is of extreme importance for the required high voltage of deposition. At too high permittivities no stable deposition is

possible. Although there is 1 ppm (at 0.3 dm^3 min^{-1}) of ozone additionally produced by the ESP in negative high voltage mode no chemical changes of the organic aerosol have been observed. Using positive high voltage the ozone production is lowered dramatically. Obviously, at these low concentrations no further modifications of the aerosol occur.

We would like to underline that the usage of this ESP is not restricted to an aerosol smog chamber experiment, but could also be used in field experiments. Further developments on ESP-ATR-FTIR spectroscopy might allow online and in situ characterization of atmospheric aerosols.

REFERENCES

Abdel-Salam, M., Nakano, M., and Mizuno, A. (2007). Electric Fields and Corona Currents in Needle-to-Meshed Plate Gaps, *J. Phys. D: Appl. Phys.* 40:3363–3370.

Allen, D. T., Palen, E. J., and Haimov, M. I. (1994). Fourier Transform Infrared Spectroscopy of Aerosol Collected in a Low Pressure Impactor (LPI/FTIR): Method Development and Field Calibration, *Aerosol Sci. Technol*. 21:325–342.

Blando, J. D., Porcja, R. J., and Turpin, B. J. (2001). Issues in the Quantitation of Functional Groups by FTIR Spectroscopic Analysis of Impactor-Collected Aerosol Samples, *Aerosol Sci. Technol.* 35:899–908.

Dekermenjian, M., Allen, D. T., Atkinson, R., and Arey, J. (1999). FTIR Analysis of Aerosol Formed in the Ozone Oxidation of Sesquiterpenes, *Aerosol Sci. Technol*. 30:349–363.

Fierz, M., Kaegi, R., and Burtscher, H. (2007). Theoretical and Experimental Evaluation of a Portable Electrostatic TEM Sampler, *Aerosol Sci. Technol*. 41:520–528.

Ghauch, A., Deveau, P.-A., Jacob, V., and Baussand, P. (2006). Use of FTIR Spectroscopy Coupled with ATR for the Determination of Atmospheric Compounds, *Talanta* 68:1294–1302.

Havers, N., Burba, P., Lambert, J., and Klockow, D. (1998). Spectroscopic Characterization of Humic-Like Substances in Airborne Particulate Matter, *J. Atmos. Chem*. 29:45–54.

Johnson, S. A., Kumar, R., and Cunningham, P. T. (1983). Airborne Detection of Acidic Sulfate Aerosol Using an ATR Impactor, *Aerosol Sci. Technol*. 2:401–405.

Keskinen, J., Janka, K., Lehtimaki, M., Graeffe, G., and Kulmala, V. (1986). Aerosol Formation Caused by Electrostatic Precipitator, *J. Aerosol Sci*. 17:647–649.

Mainelis, G., Willeke, K., Adhikari, A. Reponen, T., and Grinshpun, S. A. (2002). Design and Collection Efficiency of a New Electrostatic Precipitator for Bioaerosol Collection, *Aerosol Sci. Technol*. 36:1073–1085.

Muckenhuber, H., and Grothe, H. (2007). A DRIFTS Study of the Heterogeneous Reaction of NO_2 with Carbonaceous Materials at Elevated Temperature, *Carbon* 45:321–329.

Morrow, P. E., and Mercer, T. T. (1964). A Point-to-Plane Electrostatic Precipitator for Particle Size Sampling, *Amer. Indust. Hygiene Assoc. J.* 25:8–14.

Sax, M., Zenobi, R., Baltensperger, U., and Kalberer, M. (2005). Time Resolved Infrared Spectroscopic Analysis of Aerosol Formed by Photo-Oxidation of 1,3,5–Trimethylbenzene and Alpha–Pinene, *Aerosol Sci. Technol*. 39:822–830.

Zhang, Y., Hu, Y. A., Ding, F., and Zhao, L. (2005). FTIR-ATR Chamber for Observation of Efflorescence and Deliquescence Processes of $NaClO_4$ Aerosol Particles on ZnSe Substrate, *Chin. Sci. Bull.* 50:2149–2152.